Mechanical Bistability in Kerr-modified Cavity Magnomechanics

Rui-Chang Shen, Jie Li,* Zhi-Yuan Fan, Yi-Pu Wang,† and J. Q. You‡
Interdisciplinary Center of Quantum Information, State Key Laboratory of Modern Optical Instrumentation, and Zhejiang Province Key Laboratory of Quantum Technology and Device, School of Physics, Zhejiang University, Hangzhou 310027, China

(Received 30 June 2022; revised 29 August 2022; accepted 1 September 2022; published 13 September 2022)

Bistable mechanical vibration is observed in a cavity magnomechanical system, which consists of a microwave cavity mode, a magnon mode, and a mechanical vibration mode of a ferrimagnetic yttrium-iron-garnet sphere. The bistability manifests itself in both the mechanical frequency and linewidth under a strong microwave drive field, which simultaneously activates three different kinds of nonlinearities, namely, magnetostriction, magnon self-Kerr, and magnon-phonon cross-Kerr nonlinearities. The magnon-phonon cross-Kerr nonlinearity is first predicted and measured in magnomechanics. The system enters a regime where Kerr-type nonlinearities strongly modify the conventional cavity magnomechanics that possesses only a radiation-pressure-like magnomechanical coupling. Three different kinds of nonlinearities are identified and distinguished in the experiment. Our Letter demonstrates a new mechanism for achieving mechanical bistability by combining magnetostriction and Kerr-type nonlinearities, and indicates that such Kerr-modified cavity magnomechanics provides a unique platform for studying many distinct nonlinearities in a single experiment.

DOI: 10.1103/PhysRevLett.129.123601

Introduction.—Bistability, or multistability, discontinuous jumps, and hysteresis are characteristic features of nonlinear systems. Bistability is a widespread phenomenon that exists in a variety of physical systems, e.g., optics [1–3], electronic tunneling structures [4], magnetic nanorings [5], thermal radiation [6], a driven-dissipative superfluid [7], and cavity magnonics [8]. Its presence requires nonlinearity in the system. To date, bistability has been studied in various mechanical systems, including nano- or micromechanical resonators [9–11], piezoelectric beams [12], mechanical morphing structures [13], and levitated nanoparticles [14]. Bistable mechanical motion finds many important applications: it is the basis for mechanical switches [15,16], memory elements [17,18], logic gates [19], vibration energy harvesters [12,20], signal amplifiers [11,14], etc.

Different mechanisms can bring about nonlinearity in the system leading to bistable mechanical motion. Most commonly, a strong drive can induce bistability of a mechanical oscillator, of which the dynamics is described by the Duffing equation [11,21–23]. Mechanical bistability can also be caused by the Casimir force [9], nanomechanical effects on Coulomb blockade [10], magnetic repulsion [24], intrinsic nonlinearity in the optomechanical coupling [25], etc.

Here, we introduce a mechanism to induce mechanical bistability, distinguished from all the above mechanisms, by exploiting rich nonlinearities in the ferrimagnetic yttrium-iron-garnet (YIG) in cavity magnomechanics (CMM). In the CMM [26–29], magnons are the quanta of collective spin excitations in magnetically ordered materials, such as YIG. They can strongly couple to microwave cavity photons by the magnetic-dipole interaction, leading to cavity polaritons [30–35]. They can also couple to deformation vibration phonons of the ferrimagnet via the magnetostrictive force [26,28,36]. Such a radiation-pressure-like magnomechanical coupling provides necessary nonlinearity, enabling a number of theoretical proposals, including the preparation of entangled states [37–41], squeezed states [42–44], mechanical quantum-ground states [45–47], slow light [48,49], thermometry [50], quantum memory [51,52], exceptional points [53], and parity-time-related phenomena [54–57], etc. In contrast, the experimental studies on this system are, by now, very limited: Magnomechanically induced transparency and absorption [26] and mechanical cooling and lasing [28] have been demonstrated.

In this Letter, we report an experimental observation of bistable mechanical vibration of a YIG sphere in the CMM. We show that both the frequency and linewidth of the mechanical mode exhibit a bistable feature as a result of the combined effects of the radiation-pressure-like magnetostrictive interaction [26,28], the magnon self-Kerr [58,59], and the magnon-phonon cross-Kerr nonlinearities. Three different kinds of nonlinearities are simultaneously activated by applying a strong drive field on the YIG sphere. Their respective contributions to the mechanical frequency and linewidth are discussed.

Kerr-modified CMM.—The CMM system consists of a microwave cavity mode, a magnon mode, and a mechanical vibration mode; see Fig. 1. In the experiment, we use the

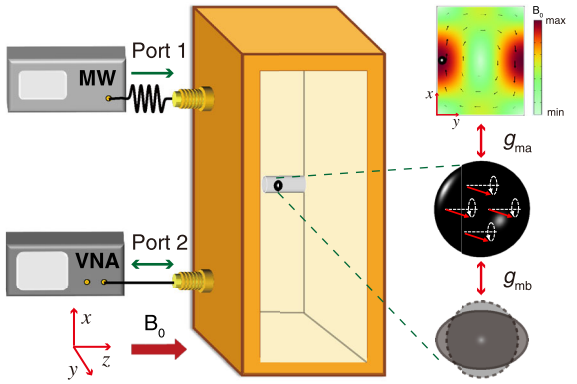

FIG. 1. Device schematic. Left panel: schematic of the CMM system. A 0.28 mm-diameter YIG sphere is placed (free to move) in a horizontal 0.9 mm-inner-diameter glass capillary and at the antinode of the magnetic field of the cavity mode TE_{101}. The cavity has two ports: Port 1 is connected to a microwave source (MW) to load the drive field, and Port 2 is connected to a vector network analyzer (VNA) to measure the reflection of the probe field with the power of −5 dBm. We set the direction of the bias magnetic field B_0 as the z direction, and the vertical direction as the x direction. Right panel: schematic of the coupled three modes.

oxygen-free copper cavity with dimensions of $42 \times 22 \times 8$ mm^3. The cavity TE_{101} mode has a frequency $\omega_a/2\pi = 7.653$ GHz, and a total decay rate $\kappa_a/2\pi = 2.78$ MHz. The cavity decay rates associated with the two ports are $\kappa_{1,2}/2\pi = 0.22$ MHz and 1.05 MHz, respectively. The magnon and mechanical modes are supported by a 0.28 mm-diameter YIG sphere. The frequency of the magnon mode can be tuned by adjusting the bias magnetic field B_0 via $\omega_m = \gamma B_0$, with γ being the gyromagnetic ratio. The magnon dissipation rate is $\kappa_m/2\pi = 2.2$ MHz. The magnon mode couples to the cavity magnetic field by the magnetic-dipole interaction with the coupling strength $g_{\rm ma}/2\pi = 7.37$ MHz, and to a vibration mode by the magnetostrictive (radiation-pressure-like) interaction with the bare magnomechanical coupling strength $g_{\rm mb}/2\pi = 1.22$ mHz. Here, we consider the lower-frequency mechanical mode (with a natural frequency $\omega_b/2\pi = 11.0308$ MHz and linewidth $\kappa_b/2\pi = 550$ Hz) in our observed two adjacent mechanical modes, which has a stronger coupling $g_{\rm mb}$. The magnomechanical coupling can be significantly enhanced by applying a pump field on the magnon mode [37]. In our experiment, this is realized by strongly driving the cavity, which linearly couples to the magnon mode. In Ref. [60], we provide a list of parameters and the details of how they are extracted by fitting the experimental data.

Under a strong pump, the Hamiltonian of the CMM system is given by [60]

$$\begin{aligned} H/\hbar = {} & \omega_a a^\dagger a + \omega_m m^\dagger m + \omega_b b^\dagger b + g_{\rm ma}(a^\dagger m + a m^\dagger) \\ & + g_{\rm mb} m^\dagger m (b + b^\dagger) + H_{\rm Kerr}/\hbar \\ & + \sqrt{\kappa_1}\varepsilon_d (a^\dagger e^{-i\omega_d t} + \text{H.c.}), \end{aligned} \tag{1}$$

where a, m, and b ($a^\dagger$, $m^\dagger$, and $b^\dagger$) are the annihilation (creation) operators of the cavity mode, the magnon mode, and the mechanical mode, respectively. The last term is the driving Hamiltonian, where κ_1 is the cavity decay rate associated with the driving port (Port 1), and $\varepsilon_d = \sqrt{P_d/(\hbar\omega_d)}$, with P_d (ω_d) being the power (frequency) of the microwave drive field. The novel part of the Hamiltonian, with respect to the conventional CMM, is the Kerr nonlinear term $H_{\rm Kerr}$ activated by the strong pump field [60],

$$H_{\rm Kerr}/\hbar = K_m m^\dagger m m^\dagger m + K_{\rm cross} m^\dagger m b^\dagger b, \tag{2}$$

where K_m is the magnon self-Kerr coefficient, and $K_{\rm cross}$ is the magnon-phonon cross-Kerr coefficient. The magnon self-Kerr effect is caused by the magnetocrystalline anisotropy [58,59], and the cross-Kerr nonlinearity originates from the magnetoelastic coupling by including the second-order terms in the strain tensor [61,62],

$$\epsilon_{ij} = \frac{1}{2}\left(\frac{\partial u_i}{\partial l_j} + \frac{\partial u_j}{\partial l_i} + \sum_k \frac{\partial u_k}{\partial l_i}\frac{\partial u_k}{\partial l_j}\right), \tag{3}$$

where u_i are the components of the displacement vector, and $l_i = i$ ($i = x, y, z$). The first-order terms lead to the conventional radiation-pressure-like interaction Hamiltonian [63], $\hbar g_{\rm mb} m^\dagger m (b + b^\dagger)$. Under a moderate drive field, the second-order terms are negligible [26,28], but can no longer be neglected when the drive becomes sufficiently strong, as in our experiment, yielding an appreciable magnon-phonon cross-Kerr nonlinearity. As will be seen later, the cross-Kerr nonlinearity is indispensable in the model for fitting the mechanical frequency shift.

Both the magnon self-Kerr and magnon-phonon cross-Kerr terms, as well as the radiation-pressure-like term, cause a magnon frequency shift $\delta\omega_m = 2K_m|M|^2 + K_{\rm cross}|B|^2 + 2g_{\rm mb}\text{Re}[B]$, where $O = \langle o \rangle$ ($o = m, b, a$) denote the average of the modes. In our experiment, the dominant contribution is from the self-Kerr nonlinearity [60], which gives a bistable magnon frequency shift [8]. Also, the cross-Kerr nonlinearity causes a mechanical frequency shift $\delta\omega_b = K_{\rm cross}|M|^2$. Using the Heisenberg-Langevin approach, we obtain the equation for the steady-state average M [60],

$$\begin{aligned} \eta_a \kappa_1 g_{\rm ma}^2 \varepsilon_d^2 = |M|^2 \Bigg[& (\Delta_m - \eta_a g_{\rm ma}^2 \Delta_a + 2K_m|M|^2)^2 \\ & + \left(\frac{\kappa_m}{2} + \eta_a g_{\rm ma}^2 \frac{\kappa_a}{2}\right)^2 \Bigg], \end{aligned} \tag{4}$$

where $\Delta_{a(m)} = \omega_{a(m)} - \omega_d$, $\eta_a = 1/[\Delta_a^2 + (\kappa_a/2)^2]$. In deriving Eq. (4), we neglect contributions from the mechanical mode to the magnon frequency shift, because of a much smaller mechanical excitation number compared

to the magnon excitation number for the drive powers used in this Letter. It is a cubic equation of the magnon excitation number $|M|^2$. In a suitable range of the drive power, there are two stable solutions, leading to the bistable magnon and phonon frequency shifts by varying the drive power.

The radiation-pressure-like coupling gives rise to an effective susceptibility of the mechanical mode [60],

$$\chi_{b,\mathrm{eff}}(\omega) = \{\chi_b^{-1}(\omega) - 2i|G_{\mathrm{mb}}|^2[\chi_{\mathrm{ma}}(\omega) - \chi_{\mathrm{ma}}^*(-\omega)]\}^{-1}, \tag{5}$$

where $\chi_b(\omega)$ is the natural susceptibility of the mechanical mode, but depends on the modified mechanical frequency $\tilde{\omega}_b = \omega_b + K_{\mathrm{cross}}|M|^2$, which includes the cross-Kerr induced frequency shift. The effective coupling $G_{\mathrm{mb}} = g_{\mathrm{mb}}M$, and $\chi_{\mathrm{ma}}(\omega) = [\chi_m^{-1}(\omega) + g_{\mathrm{ma}}^2\chi_a(\omega)]^{-1}$, where $\chi_m(\omega)$ and $\chi_a(\omega)$ are the natural susceptibilities of the magnon and cavity modes, with the magnon detuning in $\chi_m(\omega)$ modified as $\tilde{\Delta}_m = \Delta_m + 2K_m|M|^2$, which includes the dominant magnon self-Kerr induced frequency shift. See Ref. [60] for the explicit expressions of the susceptibilities.

The effective mechanical susceptibility yields a frequency shift of the phonon mode (the so-called "magnonic spring" effect [28], in analogy to the "optical spring" in optomechanics [69]),

$$\delta\omega_b = -\mathrm{Re}\{2i|G_{\mathrm{mb}}|^2[\chi_{\mathrm{ma}}(\omega) - \chi_{\mathrm{ma}}^*(-\omega)]\} + K_{\mathrm{cross}}|M|^2, \tag{6}$$

where we write together the frequency shift induced by the cross-Kerr nonlinearity. Moreover, it leads to the following mechanical linewidth change:

$$\delta\Gamma_b = \mathrm{Im}\{2i|G_{\mathrm{mb}}|^2[\chi_{\mathrm{ma}}(\omega) - \chi_{\mathrm{ma}}^*(-\omega)]\}. \tag{7}$$

Clearly, this *linewidth* change is only caused by the radiation-pressure-like coupling, distinguished from the *frequency* shift caused by the self-Kerr or cross-Kerr nonlinearity. By applying a red- or blue-detuned drive field, we can choose to operate the system in two different regimes, where either the magnomechanical anti-Stokes or Stokes scattering is dominant. This yields an increased ($\delta\Gamma_b > 0$) or a reduced ($\delta\Gamma_b < 0$) mechanical linewidth, corresponding to the cooling or amplification of the mechanical motion [28,69].

In our system, due to the strong coupling $g_{\mathrm{ma}} > \kappa_m, \kappa_a$, the magnon and cavity modes form two cavity polariton (hybridized) modes (Fig. 2, left panels) [30–35]. Here, a red (blue)-detuned drive means that the drive frequency is lower (higher) than the frequency of the cavitylike polariton mode, i.e., the "deeper" polariton in the spectra close to the cavity resonance. For the red (blue)-detuned drive, we show the anti-Stokes (Stokes) sidebands associated with two mechanical modes for two drive powers in the enlarged plots of Fig. 2(a) [Fig. 2(b)]. When the detuning between the drive field and the deeper polariton matches the mechanical frequencies, the anti-Stokes (Stokes) sidebands are manifested as the magnomechanically induced transparency (absorption) [26].

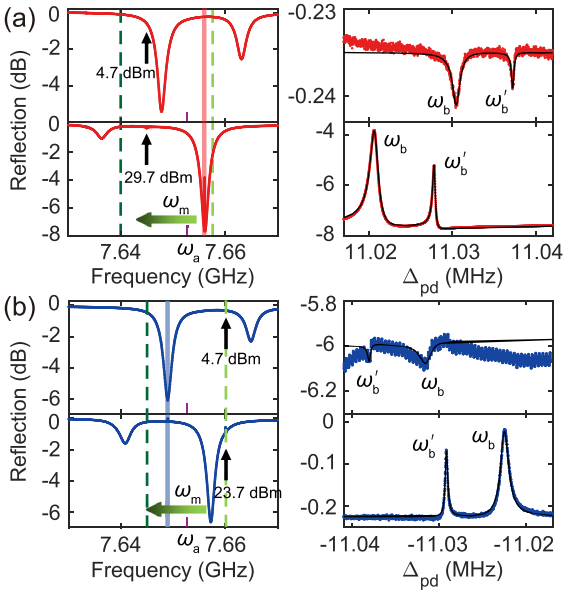

FIG. 2. (a) Left panel: measured reflection spectra under a red-detuned drive. The frequency of the drive field $\omega_d/2\pi = 7.645$ GHz (black arrow). By increasing the drive power, the magnon frequency shift is negative: $\omega_m^L/2\pi = 7.658$ GHz (light green dashed line) at a lower power $P_d = 4.7$ dBm (upper panel) and $\omega_m^H/2\pi = 7.640$ GHz (dark green dashed line) at $P_d = 29.7$ dBm (lower panel). The green arrow indicates the direction in which the magnon frequency shifts by increasing the power. Right panel: enlargement of the red shaded areas in the left panel shows detailed spectra of the magnomechanically induced resonances, where $\Delta_{\mathrm{pd}} = \omega_p - \omega_d$. The black lines are the fitting curves. (b) Left panel: measured reflection spectra under a blue-detuned drive. The drive frequency $\omega_d/2\pi = 7.660$ GHz. By adjusting the bias magnetic field, the magnon frequency is tuned close to the drive frequency $\omega_m^L/2\pi \simeq \omega_d$ at the power $P_d = 4.7$ dBm. Increasing the power to 23.7 dBm, the magnon frequency $\omega_m^H/2\pi = 7.645$ GHz. Right panel: enlargement of the blue shaded areas in the left panel shows detailed spectra of the magnomechanically induced resonances. We observe two adjacent mechanical modes with the frequencies $\omega_b/2\pi = 11.0308$ MHz and $\omega_b'/2\pi = 11.0377$ MHz. Because of their similar behaviors, we focus on the lower-frequency mode in the text.

Red-detuned drive.—To implement a red-detuned drive, we drive the cavity with a microwave field at frequency $\omega_d/2\pi = 7.645$ GHz. By adjusting the bias magnetic field, we tune the magnon frequency to be $\omega_m^L/2\pi = 7.658$ GHz at the drive power $P_d = 4.7$ dBm [see Fig. 2(a)]. We have the [110] axis of the YIG sphere aligned parallel to the static magnetic field, which yields a negative self-Kerr coefficient $K_m/2\pi = -6.5$ nHz. An increase in power

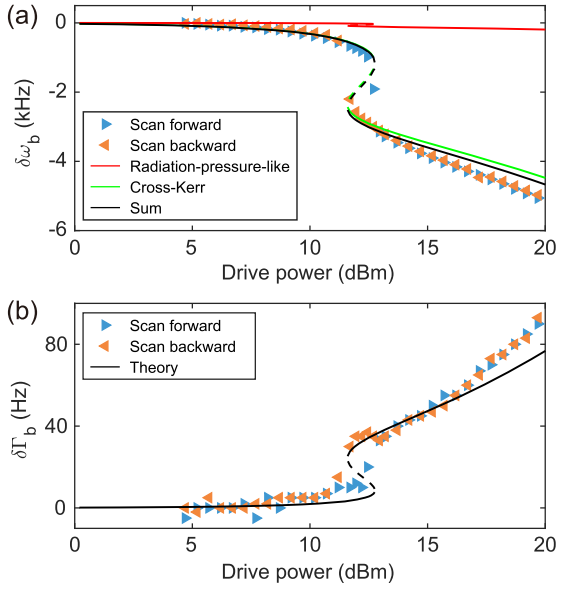

FIG. 3. Bistable mechanical frequency and linewidth under a red-detuned drive. (a) The mechanical frequency shift versus the drive power. The red (green) curve is the fitting of the frequency shift induced by the radiation-pressure-like coupling (cross-Kerr effect) using Eq. (6), and the black curve is the sum of the two contributions. (b) The mechanical linewidth variation versus the drive power. The black curve is the fitting of the linewidth change using Eq. (7). In both figures, the blue (orange) triangles are the experimental data obtained via forward (backward) sweep of the drive power.

thus results in a negative magnon frequency shift $\delta\omega_m = 2K_m|M|^2$, and the magnon frequency reduces to $\omega_m^H/2\pi = 7.640$ GHz when the power increases to $P_d = 29.7$ dBm [Fig. 2(a)], which yields an effective coupling $G_{\rm mb}/2\pi = 45.8$ kHz. Under these conditions, the magnon excitation number $|M|^2$ shows a bistable behavior through variation of the power.

Equation (6) indicates that the radiation-pressure-like coupling results in a mechanical frequency shift, and so does the cross-Kerr nonlinearity. This is confirmed by the experimental data in Fig. 3(a). It shows that the cross-Kerr plays a dominant role because of a large magnon excitation number, and both the frequency shifts caused, respectively, by the cross-Kerr and the radiation-pressure-like coupling show a bistable feature with the forward and backward sweeps of the drive power. This is because both of them originate from the bistable magnon excitation number $|M|^2$, cf. Eq. (6). Note that for the spring effect, the bistability of $|M|^2$ is mapped to the magnon frequency shift $\tilde{\Delta}_m$, then to the polariton susceptibility $\chi_{\rm ma}(\omega)$, and finally to the mechanical frequency.

By increasing the drive power from 4.7 to 19.7 dBm, the cross-Kerr causes a maximum frequency shift of -4.6 kHz [Fig. 3(a), the green line]. The fitting cross-Kerr coefficient is $K_{\rm cross}/2\pi = -5.4$ pHz. Under the red-detuned drive, the magnonic spring effect yields a negative frequency shift $\delta\omega_b = {\rm Re}[\chi_{b,\rm eff}^{-1}(\omega) - \chi_b^{-1}(\omega)] < 0$ [Fig. 3(a), the red line], and the maximum frequency shift is -200 Hz. Adding up these two frequency shifts gives the total mechanical frequency shift [Fig. 3(a), the black line], which fits well with the experimental data [Fig. 3(a), triangles] when the power is not too strong.

Another interesting finding is the bistable feature of the mechanical linewidth [Fig. 3(b)]. The magnomechanical backaction leads to the variation of the mechanical linewidth $\delta\Gamma_b = -{\rm Im}[\chi_{b,\rm eff}^{-1}(\omega) - \chi_b^{-1}(\omega)]$. For a red-detuned drive, the anti-Stokes process is dominant, resulting in an increased mechanical linewidth $\delta\Gamma_b > 0$ and the cooling of the motion. The bistable mechanical linewidth is also induced by the bistable $|M|^2$ [see Eq. (7)], similar to the mechanical frequency. The theory fits well with the experimental results, and the discrepancy appears only in the high-power regime. This is because the considerable heating effect at strong pump powers can broaden the mechanical linewidth [70,71], which is not included in our model.

Blue-detuned drive.—When a blue-detuned drive is applied, the system enters a regime where the Stokes scattering is dominant. The magnomechanical parametric down-conversion amplifies the mechanical motion with the characteristic of a reduced linewidth. Furthermore, the mechanical frequency shift induced by the spring effect will move in the opposite direction compared with the red-detuned drive.

To implement a blue-detuned drive, we drive the cavity with a microwave field at frequency $\omega_d/2\pi = 7.66$ GHz, and tune the magnon frequency close to the drive frequency [see Fig. 2(b)]. We attempted to make the Stokes sideband of the drive field resonate with the "deeper" polariton *at a high pump power*, such that the Stokes scattering rate is maximized and the magnomechanical coupling strength $G_{\rm mb}$ becomes strong. However, to meet the drive conditions for a *bistable* magnon excitation number $|M|^2$, the drive frequency is restricted to a certain range, which hinders us from making the Stokes sideband and the "deeper" polariton resonate. Therefore, we only achieve this at lower drive powers, giving a faint magnomechanically induced absorption [Fig. 2(b), upper panels].

From the red to the blue detuning, we only adjust the magnon and the drive frequencies. Because the direction of the crystal axis is unchanged, the magnon self-Kerr coefficient K_m is still negative, so again a negative frequency shift occurs by increasing the power [green arrow in Fig. 2(b)]. For the power up to 23.7 dBm, which yields $G_{\rm mb}/2\pi = 42.7$ kHz, the frequency of the cavitylike polariton is always lower than the drive frequency, so the system is operated under a blue-detuned drive.

Figure 4 displays the bistable mechanical frequency shift $\delta\omega_b$ and linewidth change $\delta\Gamma_b$. For the frequency shift, both the contributions from the cross-Kerr and the radiation-pressure-like coupling should be considered, but the former

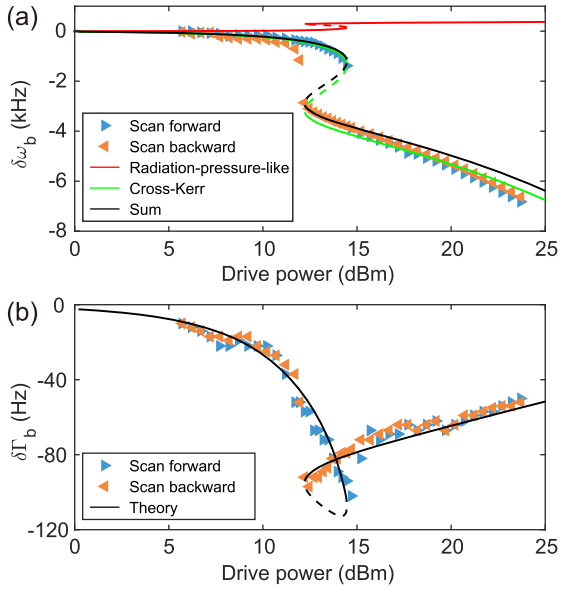

FIG. 4. Bistable mechanical frequency and linewidth under a blue-detuned drive. (a) The mechanical frequency shift and (b) the mechanical linewidth change versus the drive power. The curves and the triangles are shown in the same manner as in Fig. 3.

plays a dominant role [Fig. 4(a), the green line], as in the case of the red-detuned drive, yielding a frequency shift of −6.5 kHz at the power of 23.7 dBm. Differently, the spring effect induced frequency shift (370 Hz at 23.7 dBm) is positive [Fig. 4(a), the red line]. The opposite frequency shifts by the spring effect in the blue- and red-detuned drives agree with the finding of Ref. [28], but no bistability was observed in their work.

The reduced mechanical linewidth $\delta\Gamma_b < 0$ under a blue-detuned drive is confirmed by Fig. 4(b). However, unlike the bistable curve in the red-detuned drive case [Fig. 3(b)], $\delta\Gamma_b$ manifests the bistability in an *alpha*-shaped curve by sweeping the drive power. This is the result of the trade-off between the growing coupling strength G_{mb} (which enhances the Stokes scattering rate, yielding an increasing $|\delta\Gamma_b|$) and the larger detuning between the Stokes sideband and the "deeper" polariton [Fig. 2(b)] (which reduces the Stokes scattering rate, resulting in a decreasing $|\delta\Gamma_b|$) by raising the drive power. These two effects are balanced when the power is in the range of 12 to 15 dBm.

Conclusions.—We have observed bistable mechanical frequency and linewidth and the magnon-phonon cross-Kerr nonlinearity in the CMM system. The mechanical bistability results from the magnomechanical backaction on the mechanical mode and the strong modifications on the backaction due to the magnon self-Kerr and magnon-phonon cross-Kerr nonlinearities. The effects of the magnon self-Kerr, the magnon-phonon cross-Kerr, and the radiation-pressure-like interactions can be identified by measuring primarily the magnon frequency shift, the mechanical frequency shift, and the mechanical linewidth, respectively. The new mechanism for achieving bistable mechanical motion revealed by this Letter promises a wide range of applications, such as in mechanical switches, memories, logic gates, and signal amplifiers.

This work was supported by the National Natural Science Foundation of China (Grants No. 11934010, U1801661, 12174329, 11874249), Zhejiang Province Program for Science and Technology (Grant No. 2020C01019), and the Fundamental Research Funds for the Central Universities (No. 2021FZZX001-02).

*Corresponding author.
jieli007@zju.edu.cn
†Corresponding author.
yipuwang@zju.edu.cn
‡Corresponding author.
jqyou@zju.edu.cn

[1] P. D. Drummond and D. F. Walls, Quantum theory of optical bistability. I. Nonlinear polarisability model, J. Phys. A **13**, 725 (1980).
[2] P. D. Drummond and D. F. Walls, Quantum theory of optical bistability. II. Atomic fluorescence in a high-Q cavity, Phys. Rev. A **23**, 2563 (1981).
[3] L. A. Lugiato, Theory of optical bistability, Prog. Opt., **21**, 69 (1984) and references therein.
[4] V. J. Goldman, D. C. Tsui, and J. E. Cunningham, Observation of Intrinsic Bistability in Resonant Tunneling Structures, Phys. Rev. Lett. **58**, 1256 (1987).
[5] F. Q. Zhu, G. W. Chern, O. Tchernyshyov, X. C. Zhu, J. G. Zhu, and C. L. Chien, Magnetic Bistability and Controllable Reversal of Asymmetric Ferromagnetic Nanorings, Phys. Rev. Lett. **96**, 027205 (2006).
[6] V. Kubytskyi, S.-A. Biehs, and P. Ben-Abdallah, Radiative Bistability and Thermal Memory, Phys. Rev. Lett. **113**, 074301 (2014).
[7] R. Labouvie, B. Santra, S. Heun, and H. Ott, Bistability in a Driven-Dissipative Superfluid, Phys. Rev. Lett. **116**, 235302 (2016).
[8] Y.-P. Wang, G.-Q. Zhang, D. Zhang, T.-F. Li, C.-M. Hu, and J. Q. You, Bistability of Cavity Magnon Polaritons, Phys. Rev. Lett. **120**, 057202 (2018).
[9] H. B. Chan, V. A. Aksyuk, R. N. Kleiman, D. J. Bishop, and F. Capasso, Nonlinear Micromechanical Casimir Oscillator, Phys. Rev. Lett. **87**, 211801 (2001).
[10] S. Sapmaz, Ya. M. Blanter, L. Gurevich, and H. S. J. van der Zant, Carbon nanotubes as nanoelectromechanical systems, Phys. Rev. B **67**, 235414 (2003).
[11] R. L. Badzey and P. Mohanty, Coherent signal amplification in bistable nanomechanical oscillators by stochastic resonance, Nature (London) **437**, 995 (2005).
[12] F. Cottone, H. Vocca, and L. Gammaitoni, Nonlinear Energy Harvesting, Phys. Rev. Lett. **102**, 080601 (2009).
[13] Z. Chen, Q. Guo, C. Majidi, W. Chen, D. J. Srolovitz, and M. P. Haataja, Nonlinear Geometric Effects in Mechanical Bistable Morphing Structures, Phys. Rev. Lett. **109**, 114302 (2012).

[14] F. Ricci, R. A. Rica, M. Spasenović, J. Gieseler, L. Rondin, L. Novotny, and R. Quidant, Optically levitated nanoparticle as a model system for stochastic bistable dynamics, Nat. Commun. **8**, 15141 (2017).
[15] Q. P. Unterreithmeier, T. Faust, and J. P. Kotthaus, Nonlinear switching dynamics in a nanomechanical resonator, Phys. Rev. B **81**, 241405(R) (2010).
[16] R. J. Dolleman, P. Belardinelli, S. Houri, H. S. J. van der Zant, F. Alijani, and P. G. Steeneken, High-frequency stochastic switching of graphene resonators near room temperature, Nano Lett. **19**, 1282 (2019).
[17] R. L. Badzey, G. Zolfagharkhani, A. Gaidarzhy, and P. Mohanty, A controllable nanomechanical memory element, Appl. Phys. Lett. **85**, 3587 (2004).
[18] D. Roodenburg, J. W. Spronck, H. S. J. van der Zant, and W. J. Venstra, Buckling beam micromechanical memory with on-chip readout, Appl. Phys. Lett. **94**, 183501 (2009).
[19] D. N. Guerra, A. Bulsara, W. Ditto, S. Sinha, K. Murali, and P. Mohanty, A noise-assisted reprogrammable nanomechanical logic gate, Nano Lett. **10**, 1168 (2010).
[20] R. L. Harne and K. W. Wang, A review of the recent research on vibration energy harvesting via bistable systems, Smart Mater. Struct. **22**, 023001 (2013).
[21] J. S. Aldridge and A. N. Cleland, Noise-Enabled Precision Measurements of a Duffing Nanomechanical Resonator, Phys. Rev. Lett. **94**, 156403 (2005).
[22] R. Almog, S. Zaitsev, O. Shtempluck, and E. Buks, Noise Squeezing in a Nanomechanical Duffing Resonator, Phys. Rev. Lett. **98**, 078103 (2007).
[23] I. Katz, A. Retzker, R. Straub, and R. Lifshitz, Signatures for a Classical to Quantum Transition of a Driven Nonlinear Nanomechanical Resonator, Phys. Rev. Lett. **99**, 040404 (2007).
[24] M. López-Suárez and I. Neri, Micro-electromechanical memory bit based on magnetic repulsion, Appl. Phys. Lett. **109**, 133505 (2016).
[25] H. Seok, L. F. Buchmann, E. M. Wright, and P. Meystre, Multimode strong-coupling quantum optomechanics, Phys. Rev. A **88**, 063850 (2013).
[26] X. Zhang, C.-L. Zou, L. Jiang, and H. X. Tang, Cavity magnomechanics, Sci. Adv. **2**, e1501286 (2016).
[27] D. Lachance-Quirion, Y. Tabuchi, A. Gloppe, K. Usami, and Y. Nakamura, Hybrid quantum systems based on magnonics, Appl. Phys. Express **12**, 070101 (2019).
[28] C. A. Potts, E. Varga, V. A. S. V. Bittencourt, S. V. Kusminskiy, and J. P. Davis, Dynamical Backaction Magnomechanics, Phys. Rev. X **11**, 031053 (2021).
[29] H. Y. Yuan, Y. Cao, A. Kamra, R. A. Duine, and P. Yan, Quantum magnonics: When magnon spintronics meets quantum information science, Phys. Rep. **965**, 1 (2022).
[30] H. Huebl, C. W. Zollitsch, J. Lotze, F. Hocke, M. Greifenstein, A. Marx, R. Gross, and S. T. B. Goennenwein, High Cooperativity in Coupled Microwave Resonator Ferrimagnetic Insulator Hybrids, Phys. Rev. Lett. **111**, 127003 (2013).
[31] Y. Tabuchi, S. Ishino, T. Ishikawa, R. Yamazaki, K. Usami, and Y. Nakamura, Hybridizing Ferromagnetic Magnons and Microwave Photons in the Quantum Limit, Phys. Rev. Lett. **113**, 083603 (2014).
[32] X. Zhang, C. L. Zou, L. Jiang, and H. X. Tang, Strongly Coupled Magnons and Cavity Microwave Photons, Phys. Rev. Lett. **113**, 156401 (2014).
[33] M. Goryachev, W. G. Farr, D. L. Creedon, Y. Fan, M. Kostylev, and M. E. Tobar, High-Cooperativity Cavity QED with Magnons at Microwave Frequencies, Phys. Rev. Applied **2**, 054002 (2014).
[34] L. Bai, M. Harder, Y. P. Chen, X. Fan, J. Q. Xiao, and C. M. Hu, Spin Pumping in Electrodynamically Coupled Magnon-Photon Systems, Phys. Rev. Lett. **114**, 227201 (2015).
[35] D. Zhang, X.-M. Wang, T.-F. Li, X.-Q. Luo, W. Wu, F. Nori, and J. Q. You, Cavity quantum electrodynamics with ferromagnetic magnons in a small yttrium-iron-garnet sphere, npj Quantum Inf. **1**, 15014 (2015).
[36] C. Kittel, Interaction of spin waves and ultrasonic waves in ferromagnetic crystals, Phys. Rev. **110**, 836 (1958).
[37] J. Li, S.-Y. Zhu, and G. S. Agarwal, Magnon-Photon-Phonon Entanglement in Cavity Magnomechanics, Phys. Rev. Lett. **121**, 203601 (2018).
[38] J. Li and S.-Y. Zhu, Entangling two magnon modes via magnetostrictive interaction, New J. Phys. **21**, 085001 (2019).
[39] H. Tan, Genuine photon-magnon-phonon Einstein-Podolsky-Rosen steerable nonlocality in a continuously-monitored cavity magnomechanical system, Phys. Rev. Research **1**, 033161 (2019).
[40] M. Yu, H. Shen, and J. Li, Magnetostrictively Induced Stationary Entanglement Between Two Microwave Fields, Phys. Rev. Lett. **124**, 213604 (2020).
[41] J. Li and S. Gröblacher, Entangling the vibrational modes of two massive ferromagnetic spheres using cavity magnomechanics, Quantum Sci. Technol. **6**, 024005 (2021).
[42] J. Li, S.-Y. Zhu, and G. S. Agarwal, Squeezed states of magnons and phonons in cavity magnomechanics, Phys. Rev. A **99**, 021801(R) (2019).
[43] W. Zhang, D.-Y. Wang, C.-H. Bai, T. Wang, S. Zhang, and H.-F. Wang, Generation and transfer of squeezed states in a cavity magnomechanical system by two-tone microwave fields, Opt. Express **29**, 11773 (2021).
[44] J. Li, Y.-P. Wang, J. Q. You, and S.-Y. Zhu, Squeezing microwaves by magnetostriction, arXiv:2101.02796.
[45] M.-S. Ding, L. Zheng, and C. Li, Ground-state cooling of a magnomechanical resonator induced by magnetic damping, J. Opt. Soc. Am. B **37**, 627 (2020).
[46] Z.-X. Yang, L. Wang, Y.-M. Liu, D.-Y. Wang, C.-H. Bai, S. Zhang, and H.-F. Wang, Ground state cooling of magnomechanical resonator in $\mathcal{PT}$-symmetric cavity magnomechanical system at room temperature, Front. Phys. **15**, 52504 (2020).
[47] M. Asjad, J. Li, S.-Y. Zhu, and J. Q. You, Magnon squeezing enhanced ground-state cooling in cavity magnomechanics, arXiv:2203.10767.
[48] C. Kong, B. Wang, Z.-X. Liu, H. Xiong, and Y. Wu, Magnetically controllable slow light based on magnetostrictive forces, Opt. Exp. **27**, 5544 (2019).
[49] K. Ullah, M. Tahir Naseem, and Ö. E. Müstecaplioglu, Tunable multiwindow magnomechanically induced transparency, Fano resonances, and slow-to-fast light conversion, Phys. Rev. A **102**, 033721 (2020).

[50] C. A. Potts, V. A. S. V. Bittencourt, S. V. Kusminskiy, and J. P. Davis, Magnon-Phonon Quantum Correlation Thermometry, Phys. Rev. Applied **13**, 064001 (2020).
[51] S.-F. Qi and J. Jing, Magnon-assisted photon-phonon conversion in the presence of structured environments, Phys. Rev. A **103**, 043704 (2021).
[52] B. Sarma, T. Busch, and J. Twamley, Cavity magnomechanical storage and retrieval of quantum states, New J. Phys. **23**, 043041 (2021).
[53] T.-X. Lu, H. Zhang, Q. Zhang, and H. Jing, Exceptional-point-engineered cavity magnomechanics, Phys. Rev. A **103**, 063708 (2021).
[54] S.-N. Huai, Y.-L. Liu, J. Zhang, L. Yang, and Y.-X. Liu, Enhanced sideband responses in a $\mathcal{PT}$-symmetric-like cavity magnomechanical system, Phys. Rev. A **99**, 043803 (2019).
[55] M. Wang, D. Zhang, X.-H. Li, Y.-Y. Wu, and Z.-Y. Sun, Magnon chaos in $\mathcal{PT}$-symmetric cavity magnomechanics, IEEE Photonics J. **11**, 5300108 (2019).
[56] Y.-T. Chen, L. Du, Y. Zhang, and J.-H. Wu, Perfect transfer of enhanced entanglement and asymmetric steering in a cavity-magnomechanical system, Phys. Rev. A **103**, 053712 (2021).
[57] M.-S. Ding, X.-X. Xin, S.-Y. Qin, and C. Li, Enhanced entanglement and steering in $\mathcal{PT}$-symmetric cavity magnomechanics, Opt. Commun. **490**, 126903 (2021).
[58] Y.-P. Wang, G. Q. Zhang, D. Zhang, X. Q. Luo, W. Xiong, S. P. Wang, T. F. Li, C. M. Hu, and J. Q. You, Magnon Kerr effect in a strongly coupled cavity-magnon system, Phys. Rev. B **94**, 224410 (2016).
[59] R.-C. Shen, Y.-P. Wang, J. Li, S.-Y. Zhu, G. S. Agarwal, and J. Q. You, Long-Time Memory and Ternary Logic Gate Using a Multistable Cavity Magnonic System, Phys. Rev. Lett. **127**, 183202 (2021).
[60] See Supplemental Material at http://link.aps.org/supplemental/10.1103/PhysRevLett.129.123601 for additional proofs, which includes Refs. [26,28,61–68].
[61] L. Landau, E. Lifshitz, A. Kosevich, J. Sykes, L. Pitaevskii, and W. Reid, *Theory of Elasticity: Volume 7, Course of Theoretical Physics* (Elsevier, Amsterdam, 1986).
[62] K. S. U. Kansanen, C. Tassi, H. Mishra, M. A. Sillanpää, and T. T. Heikkilä, Magnomechanics in suspended magnetic beams, Phys. Rev. B **104**, 214416 (2021).
[63] Z.-Y. Fan, R.-C. Shen, Y.-P. Wang, J. Li, and J. Q. You, Optical sensing of magnons via the magnetoelastic displacement, Phys. Rev. A **105**, 033507 (2022).
[64] A. G. Gurevich and G. A. Melkov, *Magnetization Oscillations and Waves* (CRC, Boca Raton, FL, 1996).
[65] O. O. Soykal and M. E. Flatte, Strong Field Interactions Between a Nanomagnet and a Photonic Cavity, Phys. Rev. Lett. **104**, 077202 (2010).
[66] T. Holstein and H. Primakoff, Field dependence of the intrinsic domain magnetization of a ferromagnet, Phys. Rev. **58**, 1098 (1940).
[67] C. Kittel, Physical theory of ferromagnetic domains, Rev. Mod. Phys. **21**, 541 (1949).
[68] D. Vitali, S. Gigan, A. Ferreira, H. R. Bohm, P. Tombesi, A. Guerreiro, V. Vedral, A. Zeilinger, and M. Aspelmeyer, Optomechanical Entanglement Between a Movable Mirror and a Cavity Field, Phys. Rev. Lett. **98**, 030405 (2007).
[69] M. Aspelmeyer, T. J. Kippenberg, and F. Marquardt, Cavity optomechanics, Rev. Mod. Phys. **86**, 1391 (2014).
[70] Y. Tsaturyan, A. Barg, E. S. Polzik, and A. Schliesser, Ultracoherent nanomechanical resonators via soft clamping and dissipation dilution, Nat. Nanotechnol. **12**, 776 (2017).
[71] G. S. MacCabe, H. J. Ren, J. Luo, J. D. Cohen, H. Y. Zhou, A. Sipahigil, M. Mirhosseini, and O. Painnter, Nano-acoustic resonator with ultralong phonon lifetime, Science **370**, 840 (2020).